

BLIND COLOR DECONVOLUTION OF HISTOPATHOLOGICAL IMAGES USING A VARIATIONAL BAYESIAN APPROACH

Natalia Hidalgo-Gavira^(a), Javier Mateos^(a), Miguel Vega^(b), Rafael Molina^(a), Aggelos K. Katsaggelos^(c)

a) Dpto. de Ciencias de la Computación e Inteligencia Artificial, Universidad de Granada, Spain

b) Dpto. de Lenguajes y Sistemas Informáticos, Universidad de Granada, Spain

c) Dept. of Electrical Engineering and Computer Science, Northwestern University, Evanston, IL, USA

ABSTRACT

Whole-slide histological images are routinely used by medical doctors in diagnosis. Most of these images are stained with the very common and inexpensive hematoxylin and eosin dyes. Slide stain separation and color normalization are crucial steps within the digital pathology workflow which require a previous color deconvolution step. This image processing task is not easy, especially when working with images taken from different microscopes and slides stained in different laboratories. In this paper, based on Variational Bayes inference, an efficient new blind color deconvolution method is proposed. The new model takes into account both spatial relations among image pixels and similarity to a given reference color-vector matrix. A comparison with classical and current state-of-the-art color deconvolution algorithms, using real images with known ground truth hematoxylin and eosin values, has been carried out. This comparison has demonstrated the superiority of the proposed approach.

Index Terms— Blind color deconvolution, histopathological images, variational Bayesian approach

1. INTRODUCTION

In digital brightfield microscopy, tissues are usually stained before digitization and evaluation by pathologists. Hematoxylin and eosin (H&E) are probably the most widely used stains. Hematoxylin stains cell nuclei blue while its counter-stain eosin stains the cytoplasm and stromal components in various shades of red/pink.

While pathologists are able to visually analyze color stained images, Computer-Aided Diagnosis (CAD) systems usually make use of the concentration of each dye absorbed by the sample. Those concentrations are used by machine learning algorithms to determine the presence of cancerous cells in the tissue [1]. Color deconvolution (CD) aims at separating a color image into the concentration of each stain present in it. This is not an easy task since the exact spectral profile of the stains varies from one image to another [2]. Hence, the stain color-vector matrix, which relates the color image and the stain concentrations, often needs to be estimated for each slide. Once the stain color-vectors are calculated, the color of different images can be normalized to a target image for an easier evaluation. This is usually done by replacing the stain vectors with the target stain vectors obtained from the reference slide, and converting the calculated concentrations back to an RGB image.

One of the first CD methods was proposed by Ruifrok *et al.* [3]. It is based on converting the RGB values into their optical

density (OD) values that are linear combinations of the concentration of absorbed dyes. The values for the stain vector of each dye can be obtained by measuring the relative absorption of each color from single-stained images. This is a supervised manual process, tedious and prone to errors. The proposed set of stain color-vectors for hematoxylin, eosin and DAB stains, is calibrated for processing and digitization at the authors' laboratory. While these values are generally used, they do not take into account inter-slide variability that may result in a poor separation. Several unsupervised methods have been proposed to tackle inter-slide variability. In [1] the problem is formulated as a blind source separation one which is solved by Non-negative Matrix Factorization (NMF) and Independent Component Analysis (ICA). In [4] SVD corrected for robustness was proposed to separate H&E stained images.

More recently, in [5] the stain color vectors are estimated by projecting the input color image to the Maxwellian chromaticity plane to form clusters, each one corresponding to one stained tissue type. In [6] color normalization is performed by first deconvolving both source and target images, applying a non-linear mapping of the source to the target image channels and recombining the mapped channels into the normalized source image. To build the stain color-vector matrix, the image is segmented into background and pixels belonging to each stain using supervised relevant vector machines. The mean color of the pixels in each class is utilized as the stain color-vector. McCann *et al.* [7] extend the method in [4] by adjusting the contrast of the eosin channel and including interaction between eosin and hematoxylin in the pixels of the hematoxylin channel where the eosin value was changed. The algorithm is tested on a set of three H&E images stained and destined to create H-only and E-only images which can be used as ground-truth separated images for the H&E image. The NMF in [1] is extended in [8] with regularization and sparsity terms which aim to represent the image using fewer "active" components for better interpreting the staining of different components. A similar Sparse NMF method is proposed by Vahadane *et al.* [9] for color normalization. The use of Non-Negative Least Squares (NNLS) instead of NMF is proposed in [10] resulting in a faster and less memory demanding method. Alsubaie *et al.* [11, 12], following [13], propose the use of ICA in the wavelet domain where the independence condition among sources is relaxed. Astola [14] states that the method in [4] obtains better results applied in the linearly inverted RGB-space and not in the (logarithmically inverted) absorbency space. While most of the previously described methods use CD prior to color normalization, the method in [15] uses sparse autoencoders to normalize the input image to a target image in a fully unsupervised manner. The method cannot, however, output the separated stains.

In this paper we propose a novel Bayesian method that simul-

This work was supported in part by the Ministerio de Economía y Competitividad under contract DPI2016-77869-C2-2-R

taneously estimates the color-vector matrix and the concentration of the stains in whole-slide histological images. In the Bayesian formulation of this blind CD problem we introduce a smoothness prior model on the stain concentrations which helps to reduce the acquisition noise and takes into account the spatial relationship between adjacent pixels. We also noticed that, despite the variability among images, the color-vector matrices are often close to a commonly accepted standard matrix. Our Bayesian modelling allows us to include this additional prior knowledge on the sought after solution. Variational Bayes inference is used to provide our solution to the CD problem [16]. This approach is able to approximate the posterior distribution in problems where it is not possible to obtain a closed form for it and has been successfully used, among others, in image restoration [17], remote sensing [18], super-resolution [19, 20], multimedia problems [21], as well as medical imaging problems such as fusion [22, 23] or EEG source localization [24].

The rest of the paper is organized as follows: in the next section we formulate the problem into the Bayesian paradigm. Bayesian inference is carried out in Sect. 3 where color-vector matrix and concentrations are estimated. In Sect. 4 the proposed method is evaluated in a set of H&E stained images and its performance is compared with other state-of-the-art methods. Finally, Sect. 5 concludes the paper.

2. BAYESIAN PROBLEM FORMULATION

The RGB intensity image detected by a brightfield microscope observing a stained histological specimen slide is the $(M \times N) \times 3$ matrix, \mathbf{I} , with columns $\mathbf{i}_c = (i_{1c}, \dots, i_{MNc})^T, c \in \{R, G, B\}$ and MN the number of pixels. According to the monochromatic Beer-Lambert law [3], the *Optical Density* (OD) for channel c of the slide, $\mathbf{y}_c \in \mathbb{R}^{MN \times 1}$, is

$$\mathbf{y}_c = -\log_{10} \left(\frac{\mathbf{i}_c}{\mathbf{i}_c^0} \right), \quad (1)$$

where the division of vectors is computed element-wise, the $\log_{10}(\cdot)$ function is applied to each element of the vector, and \mathbf{i}_c^0 denotes the incident light. For a slide stained using n_s stains the observed OD image $\mathbf{Y} = [\mathbf{y}_R, \mathbf{y}_G, \mathbf{y}_B] \in \mathbb{R}^{MN \times 3}$ can be obtained from

$$\mathbf{Y}^T = \mathbf{M}\mathbf{C}^T + \mathbf{N}^T, \quad (2)$$

where \mathbf{N} is a random matrix of size $MN \times 3$ with i.i.d. $\mathcal{N}(0, \beta^{-1})$ components, $\mathbf{C} \in \mathbb{R}^{MN \times n_s}$ is the stain concentrations matrix

$$\mathbf{C} = \begin{bmatrix} c_{11} & \dots & c_{1n_s} \\ \vdots & & \vdots \\ c_{MN1} & \dots & c_{MNn_s} \end{bmatrix} = \begin{bmatrix} \mathbf{c}_{1,:}^T \\ \vdots \\ \mathbf{c}_{MN,:}^T \end{bmatrix} = [\mathbf{c}_1 \dots \mathbf{c}_{n_s}],$$

with $\mathbf{c}_{i,:}^T = (c_{i1}, \dots, c_{in_s}), i = 1, \dots, MN$ denoting the i -th row, $\mathbf{c}_s = (c_{1s}, \dots, c_{MN s})^T, s \in \{1, \dots, n_s\}$ the s -th column and $\mathbf{M} \in \mathbb{R}^{3 \times n_s}$ the normalized stains' specific color-vector matrix. Each column in matrix \mathbf{M} is a unit ℓ_2 norm stain color-vector containing the relative RGB color composition of the corresponding stain.

Color Deconvolution is a technique that allows to obtain the stain concentration matrix, \mathbf{C} , and the color-vector matrix, \mathbf{M} , from the observed optical densities, \mathbf{Y} . In this paper, a Bayesian formulation of the blind CD problem is proposed. Following the degradation

model in (2), we have

$$\begin{aligned} p(\mathbf{Y}|\mathbf{M}, \mathbf{C}) &= \prod_{i=1}^{MN} p(\mathbf{y}_{i,:}|\mathbf{M}, \mathbf{c}_{i,:}) \\ &= \prod_{i=1}^{MN} \mathcal{N}(\mathbf{y}_{i,:}|\mathbf{M}\mathbf{c}_{i,:}, \beta^{-1}\mathbf{I}_{3 \times 3}). \end{aligned} \quad (3)$$

The stain concentrations at each pixel on the image are expected to have values similar to ones of the surrounding pixels. So, we impose smoothing prior models on the concentrations \mathbf{c}_s , for $s = 1, \dots, n_s$, that is, on the columns of \mathbf{C} , as

$$p(\mathbf{C}) = \prod_{s=1}^{n_s} p(\mathbf{c}_s) \propto \prod_{s=1}^{n_s} \alpha_s^{\frac{MN}{2}} \exp\left(-\frac{1}{2}\alpha_s \mathbf{c}_s^T \mathbf{F}^T \mathbf{F} \mathbf{c}_s\right), \quad (4)$$

where $\mathbf{F} \in \mathbb{R}^{MN \times MN}$ is a smoothing filter and $\alpha_s, s = 1, \dots, n_s$, controls the amount of smoothness.

The color-vector matrix $\mathbf{M} = [\mathbf{m}_1, \dots, \mathbf{m}_{n_s}]$ is also unknown, because it depends on the staining procedures and microscopes. In [3], standard color-vectors for hematoxylin, eosin and DAB stains were proposed. Although those standard color-vectors are not usually exact for each single image, they are very representative and have been frequently used. In this paper we incorporate the similarity to a representative color-vector matrix $\underline{\mathbf{M}} = [\underline{\mathbf{m}}_1, \dots, \underline{\mathbf{m}}_{n_s}]$ into the prior model

$$p(\mathbf{M}) = \prod_{s=1}^{n_s} p(\mathbf{m}_s) \propto \prod_{s=1}^{n_s} \gamma_s^{\frac{3}{2}} \exp\left(-\frac{1}{2}\gamma_s \|\mathbf{m}_s - \underline{\mathbf{m}}_s\|^2\right). \quad (5)$$

where $\gamma_s, s = 1, \dots, n_s$, controls our confidence on the accuracy of $\underline{\mathbf{m}}_s$.

The joint probability distribution for our problem is, then, given by

$$p(\mathbf{Y}, \mathbf{C}, \mathbf{M}) = p(\mathbf{Y}|\mathbf{C}, \mathbf{M})p(\mathbf{M})p(\mathbf{C}). \quad (6)$$

3. BAYESIAN INFERENCE

Following the Bayesian paradigm, inference will be based on the posterior

$$p(\mathbf{C}, \mathbf{M}|\mathbf{y}) = \frac{p(\mathbf{y}|\mathbf{C}, \mathbf{M})p(\mathbf{M})p(\mathbf{C})}{p(\mathbf{y})} \quad (7)$$

which cannot be obtained in closed form, so a variational approach [16] has been applied.

In this paper $p(\mathbf{C}, \mathbf{M}|\mathbf{y})$ is approximated by the distribution

$$q(\mathbf{C}, \mathbf{M}) = \prod_{s=1}^{n_s} q(\mathbf{m}_s) \prod_{s=1}^{n_s} q(\mathbf{c}_s). \quad (8)$$

It can then be shown [16] that for each unknown $\theta \in \Theta = \{\mathbf{m}_1, \dots, \mathbf{m}_{n_s}, \mathbf{c}_1, \dots, \mathbf{c}_{n_s}\}$, $q(\theta)$ will have the form

$$q(\theta) \propto \exp\langle \log p(\mathbf{Y}, \mathbf{C}, \mathbf{M}) \rangle_{q(\Theta \setminus \theta)}, \quad (9)$$

where $\Theta \setminus \theta$ represents all the variables in Θ except θ . Estimates for the different variables can be obtained as $\hat{\theta} = \langle \theta \rangle_{q(\theta)}$. Let us now derive the analytic expressions for each unknown estimate.

Algorithm 1 Variational Bayesian Blind Color Deconvolution

Require: Observed image \mathbf{I} , reference color-vector matrix $\underline{\mathbf{M}}$ and parameter values β , α_s and γ_s , $s = 1, \dots, n_s$.

From \mathbf{I} obtain the observed OD \mathbf{Y} image using (1) and set $\langle \mathbf{m}_s \rangle^{(0)} = \underline{\mathbf{m}}_s$, $\Sigma_{\mathbf{m}_s}^{(0)} = \mathbf{0}$, $\forall s = 1, \dots, n_s$, and $n = 0$.

while convergence criterion is not met **do**

1. Set $n = n + 1$.
2. Using $\langle \mathbf{m}_s \rangle^{(n-1)}$ and $\Sigma_{\mathbf{m}_s}^{(n-1)}$ obtain the concentration updates $\langle \mathbf{c}_s \rangle^{(n)}$ and $\Sigma_{\mathbf{c}_s}^{(n)}$ from (15) and (14).
3. Using $\langle \mathbf{c}_s \rangle^{(n)}$ and $\Sigma_{\mathbf{c}_s}^{(n)}$ obtain the color vector update $\langle \mathbf{m}_s \rangle^{(n)}$ and $\Sigma_{\mathbf{m}_s}^{(n)}$ from (19) and (18).

end while

Output the color-vector $\hat{\mathbf{m}}_s = \langle \mathbf{m}_s \rangle^{(n)}$ and the concentrations $\hat{\mathbf{c}}_s = \langle \mathbf{c}_s \rangle^{(n)}$, $\forall s = 1, \dots, n_s$.

3.1. Stain Concentration Update

To estimate the s -th stain concentration, we remove from the observation the contribution provided by other stains, that is, we calculate

$$\mathbf{e}_{i,:}^{-s} = \mathbf{y}_{i,:} - \sum_{k \neq s} \langle c_{ik} \rangle \langle \mathbf{m}_k \rangle, \quad i = 1, \dots, MN. \quad (10)$$

Then, we define

$$z_i^{-s} = \langle \mathbf{m}_s \rangle^T \mathbf{e}_{i,:}^{-s}, \quad i = 1, \dots, MN \quad (11)$$

and, from (6) and (9), we have

$$\begin{aligned} \langle \log p(\mathbf{y}, \mathbf{C}, \mathbf{M}) \rangle_{q(\Theta \setminus \mathbf{c}_s)} &= -\frac{1}{2} \alpha_s \mathbf{c}_s^T \mathbf{F}^T \mathbf{F} \mathbf{c}_s \\ &\quad - \frac{\beta}{2} \left(\|\mathbf{c}_s\|^2 \langle \|\mathbf{m}_s\|^2 \rangle - 2 \mathbf{c}_s^T \mathbf{z}^{-s} \right) + \text{const} \end{aligned} \quad (12)$$

which produces

$$q(\mathbf{c}_s) = \mathcal{N}(\mathbf{c}_s | \langle \mathbf{c}_s \rangle, \Sigma_{\mathbf{c}_s}), \quad (13)$$

where

$$\Sigma_{\mathbf{c}_s}^{-1} = \beta \langle \|\mathbf{m}_s\|^2 \rangle \mathbf{I}_{MN \times MN} + \alpha_s \mathbf{F}^T \mathbf{F}, \quad (14)$$

$$\langle \mathbf{c}_s \rangle = \beta \Sigma_{\mathbf{c}_s} \mathbf{z}^{-s}. \quad (15)$$

3.2. Color-Vector Update

In a similar way, using (10), from (6) and (9) we now have

$$\begin{aligned} \langle \log p(\mathbf{y}, \mathbf{C}, \mathbf{M}) \rangle_{q(\Theta \setminus \mathbf{m}_s)} &= -\frac{1}{2} \gamma_s \|\mathbf{m}_s - \underline{\mathbf{m}}_s\|^2 \\ &\quad - \frac{\beta}{2} \left(\|\mathbf{m}_s\|^2 \sum_i \langle c_{is}^2 \rangle - 2 \mathbf{m}_s^T \sum_i \langle c_{is} \rangle \mathbf{e}_{i,:}^{-s} \right) + \text{const} \end{aligned} \quad (16)$$

which produces

$$q(\mathbf{m}_s) = \mathcal{N}(\mathbf{m}_s | \langle \mathbf{m}_s \rangle, \Sigma_{\mathbf{m}_s}), \quad (17)$$

where

$$\Sigma_{\mathbf{m}_s}^{-1} = (\beta \sum_i \langle c_{is}^2 \rangle + \gamma_s) \mathbf{I}_{3 \times 3}, \quad (18)$$

$$\langle \mathbf{m}_s \rangle = \Sigma_{\mathbf{m}_s} (\beta \sum_i \langle c_{is} \rangle \mathbf{e}_{i,:}^{-s} + \gamma_s \underline{\mathbf{m}}_s). \quad (19)$$

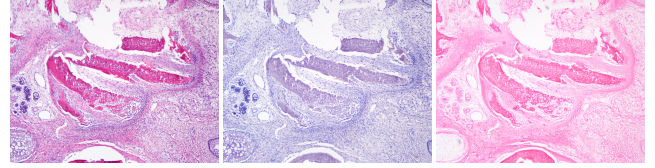


Fig. 1. Observed slide HE1 of BDSSHI [7] and its corresponding ground truth separations in hematoxylin (H1) and eosin (E1).

Notice that $\langle \mathbf{m}_s \rangle$ may not be a unitary vector but we can always replace $\langle \mathbf{m}_s \rangle$ by $\langle \mathbf{m}_s \rangle / \|\langle \mathbf{m}_s \rangle\|$ and $\Sigma_{\mathbf{m}_s}$ by $\Sigma_{\mathbf{m}_s} / \|\langle \mathbf{m}_s \rangle\|^2$. Notice also that $\langle c_{is}^2 \rangle$ can be calculated from (14) and (15) using the Fourier transform and $\langle \|\mathbf{m}_s\|^2 \rangle$ can be easily calculated from (18) and (19).

The proposed Variational Bayesian Blind Color Deconvolution method, summarized in Algorithm 1, allows to obtain the estimated concentrations $\hat{\mathbf{c}}_s$ and stain color-vector $\hat{\mathbf{m}}_s$ by iterating on the concentration and color-vector updates until convergence. Finally, an RGB image of each separated stain, $\hat{\mathbf{y}}_s^{\text{sep}}$, can be obtained as

$$\hat{\mathbf{y}}_s^{\text{sep}} = \exp_{10}(-\hat{\mathbf{m}}_s \hat{\mathbf{c}}_s^T). \quad (20)$$

4. EXPERIMENTS

The proposed algorithm has been tested on the *Benchmark Dataset for Stain Separation in Histology Images* (BDSSHI) proposed in [7]. The BDSSHI consists of three RGB images of hematoxylin & eosin stained slides, {HE1, HE2, HE3}, together with their corresponding hematoxylin-only {H1, H2, H3} and eosin-only {E1, E2, E3} stained images that can be used as ground truth for the separation process. To obtain the set of images, each slide was eosin stained, imaged, destained, hematoxylin stained, imaged, stained also with eosin and imaged. Figure 1 shows one of the microscopic images in the dataset. Note that this procedure produced some structural changes in the tissues (see, for instance, the central lower part of Fig. 1).

We set the parameters of Algorithm 1 as follows: The reference color-vector matrix $\underline{\mathbf{M}}$ is set to the one proposed in [3] for the H&E stains. For all images we selected the distribution parameters $\beta = 10$, $\alpha_1 = 8$, $\gamma_1 = 10$ (for the hematoxylin concentrations) and $\alpha_2 = 18$, $\gamma_2 = 10$ (for the eosin ones). Notice that these parameters can, in principle, be estimated within the variational framework but their estimation is proposed as future work. The algorithm was run until the convergence criterion $\|\langle \mathbf{c}_s \rangle^{(n)} - \langle \mathbf{c}_s \rangle^{(n-1)}\|^2 / \|\langle \mathbf{c}_s \rangle^{(n)}\|^2 < 10^{-5}$ was satisfied for both stains, that is, $s = 1, 2$. This is met in about 15 iterations of the algorithm.

The resulting images, one of which is shown in Fig. 2(f), show a very good stain separation. Both hematoxylin (depicted in the right hand side of the image in Fig. 2(f)) and eosin (in the left hand side) are close to the ground truth, shown in Fig. 2(a) and all the structures present in both stained images are extracted. We note that, for all tested images, the hematoxylin estimation has slightly less contrast than the ground truth and the eosin estimation, on the other hand, presents a higher contrast. We also note that the proposed method is not very sensitive to the parameter values and many combinations of them produce indistinguishable results.

The performance of the proposed method is compared with publicly available implementations of the methods in [3, 4, 7, 9], from

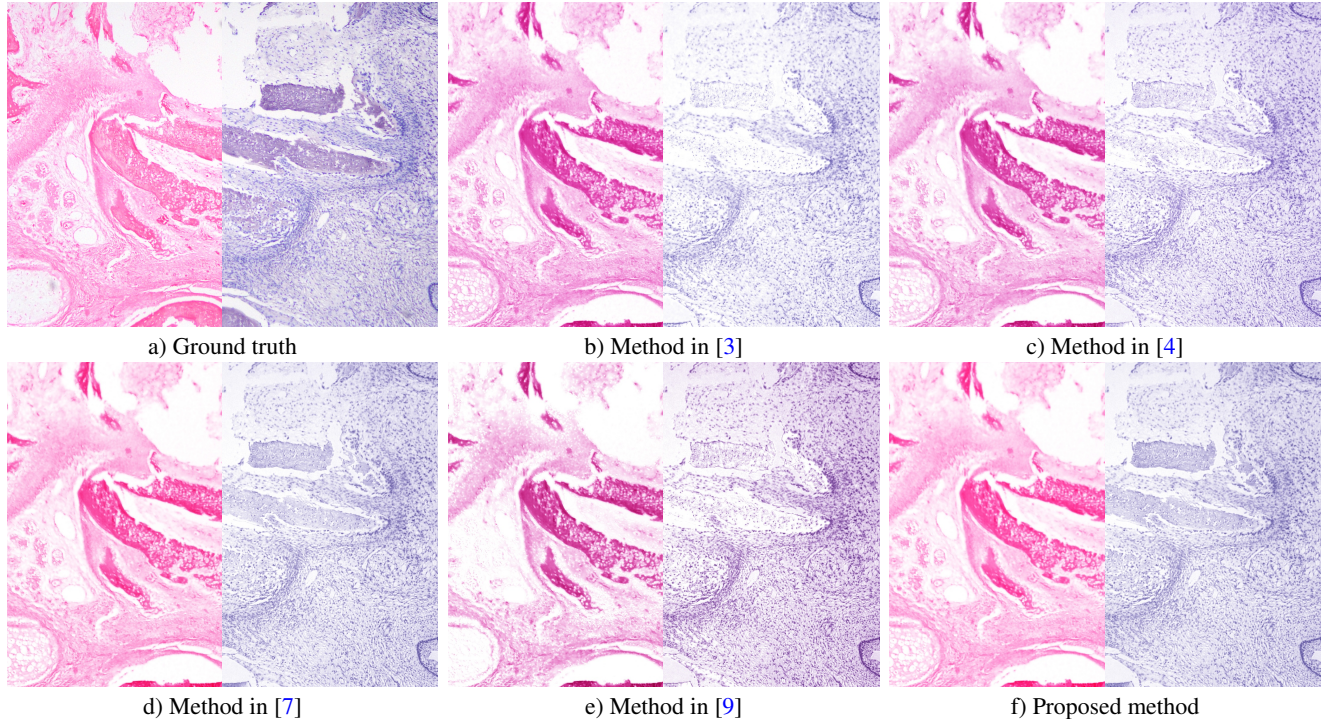


Fig. 2. Ground truth and separations for the proposed and the compared method.

classical to recent. Figure 2(b)–(d) show the stain separations obtained by those methods for the H&E image in Fig. 1. Visually, the results of the proposed method and the method in [7] are much closer to ground truth than those of the other methods. The hematoxylin shows more clearly the nuclei and the long structure in the center of the image (corresponding to bone tissue [7]). The eosin estimations obtained by the proposed method and the method in [7] are more similar to the ground truth than the other methods’ but all the estimations have higher contrast than the ground truth. The method in [7] seems to produce slightly less contrasted eosin estimation than ours. Numerical comparison is obtained by the *Peak Signal to Noise Ratio* (PSNR) measure. Due to the dataset generation process, where the tissues are stained, destained and stained again, there are slight position and shape differences between the H&E, E-only and H-only images. To minimize this effect, in [7] the ground truth images are registered to the separated ones. We used the registered images in [7] as ground truth images for the comparison. Table 1 show the figures-of-merit for the different methods. From the table it is clear that the proposed method performs better than the competitors, except for the case of the eosin stain for the algorithm in [7]. This was expected since this algorithm selectively modifies the obtained values for the stain separations to better accommodate ground truth. More precisely, in [7] the eosin separation is corrected in contrast by adding a small part of the hematoxylin stain, and the hematoxylin stain is then computed again by taking into account interaction between the stains in those places where the contrast of the eosin coefficients is adjusted. Note that, in spite of these adjustments, our proposed method provides better results for the hematoxylin stain than the method in [7]. We notice that these results are consistent for all the images in the dataset. An election of the model parameters tuned to each image may increase the reconstruction accuracy at the expense of testing more configurations.

Table 1. PSNR for the different methods and images in the dataset.

image	stain	[3]	[4]	[7]	[9]	proposed
HE1	H	17.07	17.35	18.20	16.56	18.35
	E	18.44	18.70	20.04	18.17	19.40
HE2	H	16.21	16.75	17.52	16.16	17.58
	E	17.15	17.54	19.37	17.08	18.25
HE3	H	16.89	17.33	18.54	16.53	18.58
	E	17.79	18.12	20.29	17.57	18.97

Regarding the computational cost, our non-optimized Matlab implementation takes 7.5 seconds on a i7-5550U @ 2.40GHz laptop with 16 GB RAM, while the mex-file implementation of the method in [3] took 0.5 s., the method in [4] took 0.4s., the method in [7] took 2.78s., and the method in [9] took 50.2s.

5. CONCLUSIONS

We have proposed a novel variational Bayesian blind color deconvolution method that simultaneously estimates the color-vector matrix and the concentration of the stains in histological images. The proposed model takes into account the spatial relations between pixels as well as the similarity to a standard color-vector matrix. The method is robust to different parameter values, simple to apply, and fast, especially compared with recent methods. Comparison with classical and recent methods demonstrated that the proposed method produces better results than the competitors, except for the eosin stain by the algorithm in [7] as already mentioned. Although we tested the proposed method on H&E stained images, other stains could be easily used. The method provides good results but there is still room for improvement. Future work includes the use of other prior models and automatic parameter estimation.

6. REFERENCES

- [1] A. Rabinovich, S. Agarwal, C. Laris, J. H. Price, and S. J. Belongie, "Unsupervised color decomposition of histologically stained tissue samples," in *Advances in neural information processing systems*, 2004, pp. 667–674.
- [2] C. R. Taylor and R. M. Levenson, "Quantification of immunohistochemistry—issues concerning methods, utility and semi-quantitative assessment II," *Histopathology*, vol. 49, no. 4, pp. 411–424, 2006.
- [3] A. C. Ruifrok and D. A. Johnston, "Quantification of histochemical staining by color deconvolution," *Analytical and quantitative cytology and histology*, vol. 23, no. 4, pp. 291–299, 2001.
- [4] M. Macenko, M. Niethammer, J. S. Marron, D. Borland, J. T. Woosley, X. Guan, C. Schmitt, and N. E. Thomas, "A method for normalizing histology slides for quantitative analysis," in *2009 IEEE International Symposium on Biomedical Imaging: From Nano to Macro*, 2009, pp. 1107–1110.
- [5] M. Gavrilovic, J. C. Azar, J. Lindblad, C. Wählby, E. Bengtsson, C. Busch, and I. B. Carlom, "Blind Color Decomposition of Histological Images," *IEEE Transactions on Medical Imaging*, vol. 32, no. 6, pp. 983–994, June 2013.
- [6] A. M. Khan, N. Rajpoot, D. Treanor, and D. Magee, "A Non-linear Mapping Approach to Stain Normalization in Digital Histopathology Images Using Image-Specific Color Deconvolution," *IEEE Transactions on Biomedical Engineering*, vol. 61, no. 6, pp. 1729–1738, June 2014.
- [7] M. T. McCann, J. Majumdar, C. Peng, C. A. Castro, and J. Kovačević, "Algorithm and benchmark dataset for stain separation in histology images," in *IEEE International Conference on Image Processing (ICIP)*, 2014, pp. 3953–3957.
- [8] J. Xu, L. Xiang, G. Wang, S. Ganesan, M. Feldman, N. N. C. Shih, H. Gilmore, and A. Madabhushi, "Sparse Non-negative Matrix Factorization (SNMF) based color unmixing for breast histopathological image analysis," *Computerized Medical Imaging and Graphics*, vol. 46, pp. 20–29, Dec. 2015.
- [9] A. Vahadane, T. Peng, A. Sethi, S. Albarqouni, L. Wang, M. Baust, K. Steiger, A. M. Schlitter, I. Esposito, and N. Navab, "Structure-preserving color normalization and sparse stain separation for histological images," *IEEE Transactions on Medical Imaging*, vol. 35, no. 8, pp. 1962–1971, Aug. 2016.
- [10] D. Carey, V. N. Wijayathunga, A. J. Bulpitt, and D. Treanor, "A novel approach for the colour deconvolution of multiple histological stains," in *Proceedings of the 19th Conference of Medical Image Understanding and Analysis*, 2015, pp. 156–162.
- [11] N. Alsubaie, S. E. A. Raza, and N. Rajpoot, "Stain deconvolution of histology images via independent component analysis in the wavelet domain," in *2016 IEEE 13th International Symposium on Biomedical Imaging (ISBI)*, 2016, pp. 803–806.
- [12] N. Alsubaie, N. Trahearn, S. E. A. Raza, D. Snead, and N. M. Rajpoot, "Stain deconvolution using statistical analysis of multi-resolution stain colour representation," *PLOS ONE*, vol. 12, no. 1, pp. e0169875, Jan. 2017.
- [13] N. Trahearn, D. Snead, I. Cree, and N. Rajpoot, "Multi-class stain separation using independent component analysis," in *Medical Imaging 2015: Digital Pathology*, 2015, p. 94200J.
- [14] L. Astola, "Stain separation in digital bright field histopathology," in *2016 Sixth International Conference on Image Processing Theory, Tools and Applications (IPTA)*, 2016, pp. 1–6.
- [15] A. Janowczyk, A. Basavanthally, and A. Madabhushi, "Stain normalization using sparse autoencoders (StaNoSA): Application to digital pathology," *Computerized Medical Imaging and Graphics*, vol. 57, pp. 50–61, 2017.
- [16] C. Bishop, *Pattern Recognition and Machine Learning*, pp. 454–455, Springer, 2006.
- [17] P. Ruiz, X. Zhou, J. Mateos, R. Molina, and A. K. Katsaggelos, "Variational Bayesian blind image deconvolution: A review," *Digital Signal Processing*, vol. 47, pp. 116–127, Dec. 2015.
- [18] V. F. Rodríguez-Galiano, E. Pardo-Igúzquiza, M. Chica-Olmo, J. Mateos, J. P. Rigol-Sánchez, and M. Vega, "A comparative assessment of different methods for Landsat 7 ETM+ pansharpening," *International Journal of Remote Sensing*, vol. 33, no. 20, pp. 6574–6599, Oct. 2012.
- [19] S. Villena, M. Vega, R. Molina, and A. K. Katsaggelos, "A non-stationary image prior combination in super-resolution," *Digital Signal Processing*, vol. 32, pp. 1–10, Sept. 2014.
- [20] S. D. Babacan, R. Molina, and A. K. Katsaggelos, "Variational Bayesian super resolution," *IEEE Transactions on Image Processing*, vol. 20, no. 4, pp. 984 – 999, 2011.
- [21] Z. Chen, S. D. Babacan, R. Molina, and A. K. Katsaggelos, "Variational Bayesian methods for multimedia problems," *IEEE Transaction on Multimedia*, vol. 16, no. 4, pp. 1000–10017, 2014.
- [22] M. Luessi, S. D. Babacan, R. Molina, J. R. Booth, and A. K. Katsaggelos, "Variational Bayesian causal connectivity analysis for fmri," *Frontiers in Neuroinformatics*, doi: 10.3389/fninf.2014.00045, vol. 8, no. 45, 2014.
- [23] M. Luessi, S.D. Babacan, R. Molina, J.R. Booth, and A. K. Katsaggelos, "Bayesian symmetrical EEG/fMRI fusion with spatially adaptive priors," *NeuroImage*, vol. 55, no. 1, pp. 113–132, Nov. 2011.
- [24] J. M. Cortes, A. Lopez, R. Molina, and A. K. Katsaggelos, "Variational Bayesian localization of EEG sources with generalized Gaussian priors," *The European Physical Journal Plus*, vol. 127, no. 11, pp. 140, 2012.